Spatial assessment of intertidal seagrass meadows using optical imaging systems and a lightweight drone

James P. Duffy[1]*, Laura Pratt[2,3], Karen Anderson[1], Peter E. Land[4], & Jamie D. Shutler[5]

1. Environment and Sustainability Institute, University of Exeter, Penryn Campus, Penryn, Cornwall, TR10 9FE, UK

2. Project Seagrass, Sustainable Places Research Institute, Cardiff University, Cardiff, CF10 3BA, UK

3. School of Biosciences, Cardiff University, The Sir Martin Evans Building, Museum Avenue, Cardiff, CF10 3AX, UK

4. Plymouth Marine Laboratory, Prospect Place, The Hoe, Plymouth, PL1 3DH, UK

5. Centre for Geography, Environment and Society, University of Exeter, Penryn Campus, Penryn, Cornwall, TR10 9FE, UK

*Corresponding author: James P. Duffy

Telephone: +44 (0) 1326 259490

E-mail: james.philip.duffy@gmail.com

Abstract

Seagrass ecosystems are highly sensitive to environmental change. They are also in global decline and under threat from a variety of anthropogenic factors. There is now an urgency to establish robust monitoring methodologies so that changes in seagrass abundance and distribution in these sensitive coastal environments can be understood. Typical monitoring approaches have included remote sensing from satellites and airborne platforms, ground based ecological surveys and snorkel/scuba surveys. These techniques can suffer from temporal and spatial inconsistency, or are very localised making it hard to assess seagrass meadows in a structured manner. Here we present a novel technique using a lightweight (sub 7 kg) drone and consumer grade cameras to produce very high spatial resolution (~4 mm pixel^{-1}) mosaics of two

intertidal sites in Wales, UK. We present a full data collection methodology followed by a selection of classification techniques to produce coverage estimates at each site. We trialled three classification approaches of varying complexity to investigate and illustrate the differing performance and capabilities of each. Our results show that unsupervised classifications perform better than object-based methods in classifying seagrass cover. We also found that the more sparsely vegetated of the two meadows studied was more accurately classified - it had lower root mean squared deviation (RMSD) between observed and classified coverage (9 to 9.5 %) compared to a more densely vegetated meadow (RMSD 16 to 22 %). Furthermore, we examine the potential to detect other biotic features, finding that lugworm mounds can be detected visually at coarser resolutions such as 43 mm pixel^{-1}, whereas smaller features such as cockle shells within seagrass require finer grained data (< 17 mm pixel^{-1}).

Highlights

- Drone based optical data collection of seagrass meadows is demonstrated.
- Ecological quadrat data was used to validate aerial data.
- Unsupervised k-means and semi-automatic object-based classification approaches were applied to the optical imaging data to map seagrass extent.
- The more sparsely vegetated meadow had lower RMSD than a dense meadow.
- Addition of texture did not greatly improve RMSD, and actually increased it in some classifications.

Keywords

Drone; Eelgrass; Monitoring; *Zostera*; Unmanned Aerial Vehicle (UAV); Remote Sensing; Classification

1. Introduction

Seagrass ecosystems have a global distribution, and they play an integral role in delivering multiple ecosystem services to coastal regions (Barbier et al., 2011; Orth et al., 2006), including the provision of nursery ground for commercial fish species (Beaumont et al., 2008; Bertelli and Unsworth, 2014), sediment stabilization (McGlathery et al., 2012), pathogen reduction in coastal waters (Lamb et al., 2017) and carbon sequestration (Fourqurean et al., 2012; Macreadie et al., 2014). Despite their evident ecological importance, seagrass ecosystems have been in decline for three decades (Waycott et al., 2009), with one in five seagrass-habitat associated species at some risk of extinction according to International Union for the Conservation of Nature (IUCN) categorisation (Short et al., 2011). With threats such as human disturbance (e.g. mechanical damage and release of toxic compounds (Short and Wyllie-Echeverria, 1996)), changes in water quality

(Duarte, 2002) and warming of seas (Marbà and Duarte, 2010) likely causing such declines, there is a clear need to develop methods to monitor the extent and health of seagrass meadows.

Monitoring efforts to date have been conducted using a range of *in situ* approaches, including scuba/snorkelling surveys (Gotceitas et al., 1997), ground-based sampling (Moore et al., 2000), and hovercraft-based mapping (Mckenzie, 2003). Active and passive remote sensing approaches are also used frequently to estimate the coverage and quality of seagrass habitats. Using active acoustic remote sensing methods such as side scan sonar, it has been shown to be possible to quantify the coverage of seagrass meadows (Barrell et al., 2015; Hossain et al., 2014), whilst passive spectral sensors on-board platforms such as satellites or light aircraft have proven useful for quantifying seagrass meadow dynamics (e.g. Baumstark et al., 2016 and Cunha et al., 2005). For example, using freely available multi-spectral Landsat data (with a spatial resolution of ~30 m per pixel), changes in seagrass meadow extent have been charted (Knudby et al., 2010), and so have fluctuations in biomass (Misbari and Hashim, 2016). Finer spatial resolution optical and infra-red satellite data from systems such as IKONOS and Quickbird (with a spatial resolution finer than 4 m) have also generated useful biomass estimates for multiple seagrass species (Lyons et al., 2015; Roelfsema et al., 2014). Beyond the commonly used four-band spectral approach (blue, green, red, infra-red), multi-spectral data with 16 spectral bands have been captured from airborne sensors and used to estimate seagrass coverage, biomass and species composition (Phinn et al., 2008). The limit of many such remote sensing techniques is the spatial resolution, which restricts the focus of studies to identification and mapping of seagrass areal extent only: even in fine spatial resolution satellite data, individual seagrass plants or shoots cannot be resolved. Additionally, the ability to detect features such as seagrass from satellite observations is frequently affected by cloud cover and variable tide states (Stekoll et al., 2006), limiting the utility and applicability of such data for time-series investigations. Furthermore, the inability of satellite measurements to capture the fine spatial patterns in the distribution of plants and biomass within seagrass meadows, particularly in sparsely vegetated areas (Valle et al., 2015), means that current scientific understanding of seasonal growth patterns and the causes of meadow decline is highly uncertain.

The recent rapid growth in deployment of lightweight low-cost drone technology has been mooted as a revolutionary addition to the toolkit of ecological and environmental researchers (Anderson and Gaston, 2013). Drones offer a low-flying platform from which fine-grained (sub-decimetre spatial resolution) remote sensing observations can be captured, and such approaches are already being used widely in fields such as

hydrology (DeBell et al., 2015), forestry science (Inoue et al., 2014), polar studies (Ryan et al., 2015) and wildlife monitoring (Chabot et al., 2015; Hodgson et al., 2013). The flexibility of the lightweight drone platform, both in deployment capabilities and customization (i.e. payload options) has led to their utilisation in coastal environments including studies monitoring beach and dune topography (Gonçalves and Henriques, 2015), classifying habitats used as nurseries for fish (including seagrass) (Ventura et al., 2016) and mapping coral reefs (Chirayath and Earle, 2016). Additionally, the self-service nature of data collection and the ability to replicate data collection with the aid of GPS navigation, make drones very useful tools for monitoring dynamic environments such as the intertidal zone. In environments such as this, other remote sensing technologies, such as low spatial resolution satellite sensors, find retrievals challenging. Reasons for this may include a large temporal gap between image acquisitions, fixed orbit patterns causing data capture at different tidal states and therefore differing effects from the water column, presence of sun glint (Kay et al., 2009), mixed pixels (Suominen and Tolvanen, 2016) and land-sea adjacency issues (Sterckx et al., 2011).

Given the extensive loss of seagrass in the British Isles in recent years (Jones and Unsworth, 2016), developing new and scale-appropriate methods for quantifying and monitoring changes in this ecosystem should improve the way that drivers of change are understood, and allow for improved management. The work presented herein uses a lightweight drone fitted with consumer grade cameras to capture aerial data of intertidal seagrass (*Zostera noltii*) meadows at low tide. We explicitly sought to address the following research questions:

i) Can a consumer grade camera and lightweight drone be used to collect proximal remote observations of intertidal seagrass meadows?
ii) How effective are different image classification techniques for mapping the distribution of intertidal *Zostera noltii* meadows?
iii) How accurate are *Zostera noltii* coverage estimates derived from drone-based photographic data?
iv) Are other biotic features (e.g. gastropod shells and lugworm mounds) detectable in the image data?

The study utilised two intertidal seagrass meadow sites with differing plant density to test a further question:

v) To what extent can the drone-based methodology capture differences in plant density using a standardised survey protocol?

In this manuscript, we demonstrate a full workflow including data capture, processing and some example classification schemes, and combine this information to obtain meadow coverage estimates at two intertidal seagrass meadow sites in Wales, UK.

2. Methods

2.1. Study Species: *Zostera noltii*

Zostera noltii (commonly known as dwarf eelgrass) has an extensive distribution, and it is found throughout the British Isles, parts of Scandinavia, the western Mediterranean, parts of west and north Africa and in the Black Sea (Pergent-Martini et al., 2015). Although assigned a status of 'Least Concern' on the IUCN red list, the overall population status is assumed to be declining (Short et al., 2010). Furthermore, apart from reports of meadow expansion in Wales (Bertelli et al., 2017), local declines in Europe have been observed in recent decades, e.g. in France (Bernard et al., 2007), the Wadden Sea (Philippart and Dijkema, 1995), Spain (Hernandez et al., 1997) and Portugal (Martins et al., 2005).

Like many seagrass species, *Z. noltii* grows in an ecological niche, requiring specific environmental conditions (e.g. substrate slope and grain size Valle et al., 2011) to successfully grow and survive. It is easily disrupted by changes in water quality and light attenuation in the water column. Multiple studies have found that sediment input into *Zostera noltii* habitat has detrimental effects on shoot density and ultimately survival, both *in-situ* (Han et al., 2012) and in a laboratory setting (Cabaço et al., 2007).

2.2. Study sites

The research was focused on two sites in Pembrokeshire in Wales, the United Kingdom (Fig. 1) both of which have *Zostera noltii* meadows. One of the meadows is located in Angle Bay (51°40'50.42"N; 5°02'35.10"W) and the other at Garron Pill (51°44'05.80"N; 4°52'55.39"W). Angle Bay is an extensive intertidal habitat covering approximately 2 km^2 at low tide. *Zostera noltii* grows in the majority of this area and was particularly dense at the time of data collection (mean percentage cover of quadrats was 54% in July 2016). The sediment at the site is relatively firm and therefore accessible (although not easily so) on foot at low tide. Garron Pill is

a more sheltered site located further upstream along the Pembroke River. It is one of several tidal inlets in the area, and when drained at low tide reveals an intertidal habitat of approximately 0.5 km^2. Seagrass was less dense at this site (mean percentage cover of quadrats was 17.6%) There is also a mixture of macroalgae-dominated, and salt marsh habitats at this site. The sediment is much less stable than at Angle Bay, and therefore only small sections of the site were accessible on foot. One plot (of approximately 50 m^2 in size) was surveyed at each site (Angle Bay and Garron Pill).

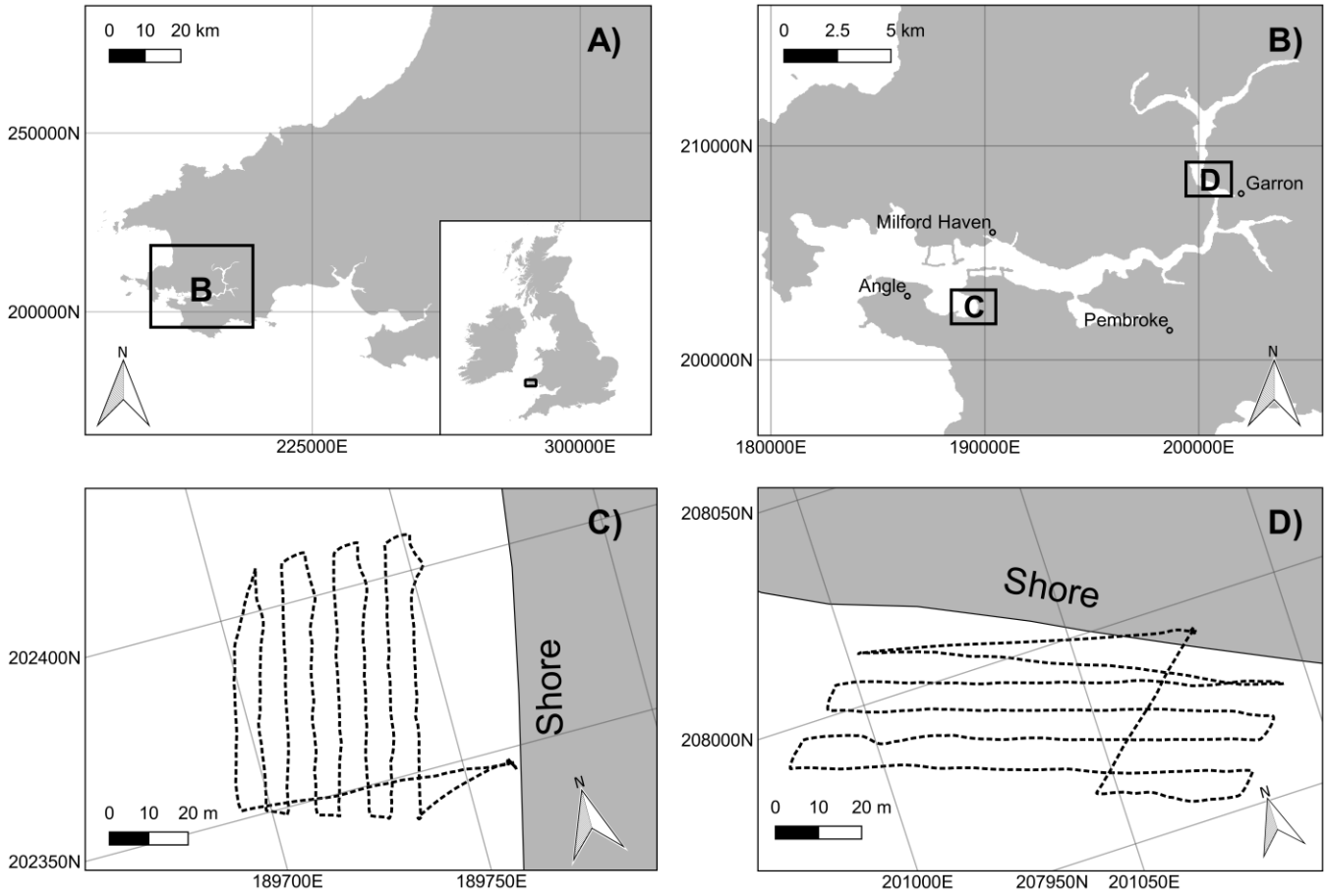

Figure 1: The location of the study sites within the context of the west Wales, UK A) and Pembrokeshire B). Flight paths are shown with dashed lines for Angle Bay C) and Garron Pill D).

2.3. Drone & Sensor Equipment

A 3D Robotics Solo (https://3dr.com/) multi-rotor drone was used with a custom designed vibration-dampened 3D-printed sensor mount (by the author JPD) (http://www.thingiverse.com/thing:1964056). The mount allowed for the attachment of a nadir-viewing Ricoh GR II compact digital camera that captures images with 16.2 effective megapixels and encompasses a complementary metal-oxide semiconductor (CMOS) sensor and prime lens with a fixed focal length of 28 mm. It can capture images in both uncompressed (RAW) and lossy (JPEG) formats, and also includes a built-in intervalometer. This allows the shutter to capture images

at given time intervals, which is useful for data capture from autonomous vehicles such as lightweight drones. Camera specifications can be found in table S1. In combination with flight planning software, ideal intervals can be calculated based on the sensors field of view, altitude and flight speed, allowing optimal image overlap to be determined, thus permitting production of good quality orthomosaics and digital terrain models (Dandois et al., 2015).

Arducopter firmware (APM:Copter solo-2.0.20) running on the Pixhawk 2 autopilot system located inside the drone allows for waypoint-guided flights. Control over position (in all three dimensions) and speed of the vehicle allow for structured surveying with user-dictated overlaps in the image data given the altitude of the drone and the field of view of the sensor. Flight missions (i.e. way point guided flight paths) were designed in Mission Planner (Oborne, 2016) and in the field, flights were conducted using the Android application Tower (Huya-Kouadio, 2016).

At both sites, two flights were conducted at 15 m altitude and a speed of 2 ms^{-1} (Fig. 1C & 1D). This altitude gave a ground sampling distance of ~4 mm when using the Ricoh GR II sensor (see Table S1). The speed and altitude combinations provided sufficient overlap (~70% frontlap and ~70% sidelap) between each image so that image matching and mosaicking was optimised. Further details of the mosaicking process can be found in section 2.5: Processing and Analysis. At Angle Bay, the data collection flight was undertaken at 16:30 GMT on 21/07/2016. Weather conditions were dry, with windspeeds averaging 4.5 ms^{-1} , light cloud cover and intermittent sunshine. At Garron Pill, the flight was conducted at 14:00 GMT on 23/07/2016. Weather conditions were dry with windspeeds averaging 7.5 ms^{-1}, and it was generally overcast. An additional two flights at 50 m altitude were undertaken at Garron Pill with an AgroCam RGB sensor (ground sampling distance of ~14 mm; Table S1), with the aim of capturing data to identify meadow boundaries. More details about these flights can be found in the supplementary information (section 1.1).

2.4. Ground Based Surveys

Quadrat sampling was used to collect *in situ* information about the seagrass meadows so that drone-based observations could be validated (Fig. 2). Twenty-seven 500 mm x 500 mm quadrats were randomly placed in each of the two ~50 m^2 plots. The following observations were recorded for each quadrat by the author (LP) trained in conducting the standard Seagrass-Watch protocols (Mckenzie et al., 2003): estimated percentage cover, shoot lengths and densities, estimated number of gastropods and algal/epiphytic cover.

We acknowledge that these estimations have their own inherent uncertainties, but for the purpose of this study assume they are truth in order to evaluate the image classification procedures presented.

Given the very high spatial resolution data capture capabilities of the camera payload on board the drone, high precision ground-truth data were required so as to georectify resulting orthomosaics and accurately locate quadrat sampling areas and features of interest within the study sites (Cunliffe et al., 2016). The position of all four quadrat corners were recorded with approximately 10 mm accuracy in *x,y,z* dimensions using a differential Global Navigation Satellite System (D-GNSS) Leica GS-08 plus survey system (comprising a base and rover). To assist with the mosaicking process, chequered targets (300 × 300 mm in size) were used as ground control points, placed at ~25 m intervals around the perimeter of the ~50 m^2 study areas (Fig 3C). To secure them in the soft substrate, two metal pegs were used on opposite corners. A laminated A4 sheet with a unique letter of the alphabet was pegged next to each target to assist in identification within the aerial photographs. Due to the shape of the plots at each site, 8 ground control points were used at Angle Bay, and 10 at Garron Pill. The central points of these black and white targets were recorded as the exact ground control points using the Leica GS-08 plus survey system.

2.5. Processing & Analysis

Photogrammetric workflows have emerged as the most popular way to collate and stitch aerial photographic image data into georectified orthomosaics (Gross and Heumann, 2016; Smith et al., 2015). For this study, Agisoft Photoscan (v 1.2.5) (Agisoft LLC, 2016) was used to generate orthomosaic models from the aerial data collected, using the positions of the ground control markers to optimize camera positions during the point cloud formation stage. They were also used to orientate and georeference the data.

The very high spatial resolution and spectral complexity of the data makes classification challenging, because of the “H resolution” problem as defined by Strahler et al. (1986). Coupled with the multitude of techniques developed for analysing and classifying cover types using optical remote sensing data, an aim of this paper was to explore three methods with differing complexity for image-based classification. In turn, we demonstrate the potential use and application of these drone-based optical imaging data for seagrass meadow assessment.

The varying complexities in the three techniques used in this study give an overview of approaches commonly used in remote sensing analyses. First, we explored the use of a basic unsupervised optical classification,

which is the simplest of approaches. Using only the red, green and blue spectral bands from the camera, we show what can be achieved with minimal processing of the data once it has been stitched via photogrammetry workflow. Building on this, we explored the effect of adding optical texture layers to the unsupervised classification workflow. This process shows that more information can be derived (than just the red, green and blue bands) from data captured with consumer grade cameras, that can in turn potentially help discriminate seagrass from its surrounding environment. Third, object-based techniques are increasingly applied to segment and classify very fine spatial resolution data. This is because objects of interest are constructed of multiple pixels as opposed to the representation of multiple objects within a single pixel (Myint et al., 2011), as is the case with coarser spatial resolution data. Given the fine spatial resolution of our data, we applied object based image analysis (OBIA) as a third classification approach (containing a 'supervised' stage) to determine whether this could be used to meaningfully improve the quality of the seagrass mapping products. We purposefully did not try to use a pixel-based supervised classifier to produce the mapping products because this would rely on the identification of individual 'pure' pixels containing either seagrass or bare substrate. Due to the data having a spatial resolution of less than 1 cm per pixel, we considered it a more robust approach to test a supervised classification that first used a segmentation algorithm to automate the identification of clusters of pixels that had similar spectral properties. A schematic describing data collection, processing and analysis is shown in Fig. 2. The classifications used are described in the following sections.

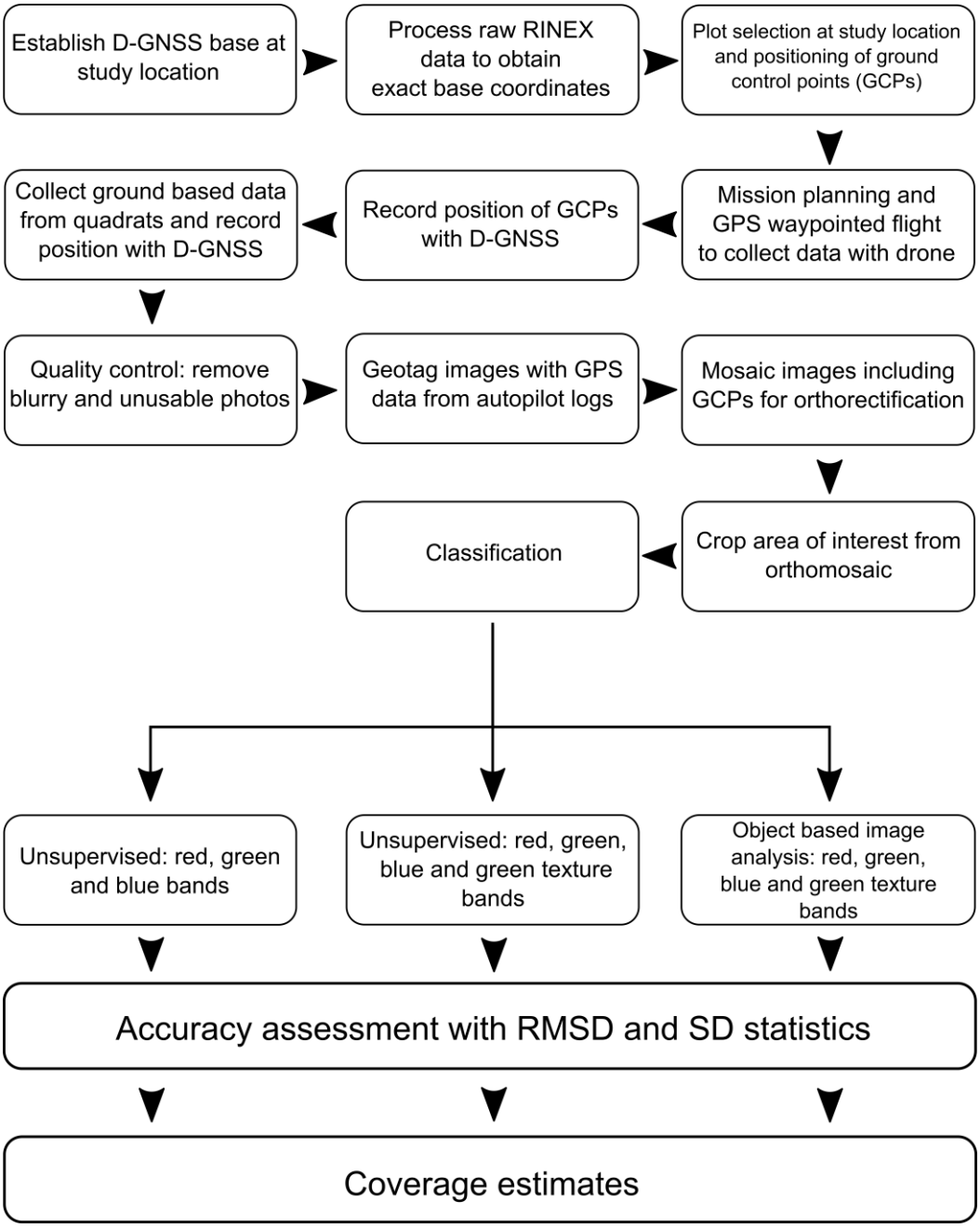

Figure 2: Data collection, processing and analysis workflow.

2.5.1. Unsupervised Classification with Optical Bands

The first type of classification performed incorporated the red, green and blue (RGB) spectral bands. An unsupervised approach using K-means (Hartigan-Wong algorithm; Hartigan and Wong, 1979) clustering was performed using the `unsuperClass` function in the `RStoolbox` (Leutner and Horning, 2016) package in R (R Core Team, 2016). Maps with two, three, four and five discreet classes were produced for each site. These classes represented seagrass and non-seagrass cover types (e.g. substrate and macroalgae). Where more than two classes were used, they were combined to create a binary result. Next, the areas coinciding with quadrat placement were extracted, and pixel counts recorded. Every possible combination of the discreet

classes was tested, and that with the lowest RMSD score when comparing classified and observed seagrass coverage was then chosen as the best candidate classifier for each site.

2.5.2. Unsupervised Classification with Optical Bands and Texture

Further to the spectral data alone, textural bands were also added to the classification process. Image texture can be used to describe patterns in images that are naturally identified and interpreted by humans but more difficult for computers to understand. Given that the dominant colour of seagrass is green, texture layers were calculated for this band only. Textural layers were calculated using moving windows on spectral data (Haralick et al., 1973). Grey level co-occurrence matrices were calculated for each orthomosaic using the `glcm` (Zvoleff, 2016) package in R (R Core Team, 2016) with a window size of 3 × 3 pixels. From these matrices, eight different measures were calculated (mean, variance, homogeneity, contrast, dissimilarity, entropy, second moment and correlation). Next, every possible combination of these layers were combined with the RGB layers, and two, three, four and five class unsupervised classifications (as described in section 2.5.1) were performed. The same selection procedure to find the combination with the lowest RMSD was followed as was performed with optical bands.

2.5.3. Segmentation & Support Vector Machine Classification

The third classification approach used the method of OBIA. This technique has seen increasing usage in the analysis of remote sensing data (Blaschke, 2010). A typical OBIA workflow involves firstly image segmentation and secondly classification of the segmented data (Myint et al., 2011). In order to keep the analysis of these data as open-source and replicable as possible, the `i.segment.uspo`, `i.segment` and `i.segment.stats` and 'v.class.mlR' functions were used in the Geographic Resources Analysis Support System (GRASS) 7.0 (GRASS Development Team, 2015) software package. Both the optical and optimum texture layers were used in these classifications. Each orthomosaic was segmented and classified with supervised training data (subset from the segmented data). Given the knowledge obtained from visual inspection of the mosaics, a two-class classification (seagrass and substrate) was applied to data from Angle Bay and five-class (seagrass, substrate, macroalgae species 1, macroalgae species 2, rock) classification for Garron Pill.

More detailed information on the OBIA procedures used can be found in the supplementary information (section 1.2).

2.5.4. Analysis of Classified Maps

All analysis of classified maps and graphing of data took place in the statistical package R 3.3.1 (R Core Team, 2016). Data manipulation and analysis were conducted using the dplyr (Wickham and Francois, 2016), raster (Hijmans, 2015) and tidyr (Wickham, 2017) packages. Graphs were created using ggplot2 (Wickham, 2009) and gridExtra (Auguie, 2016).

Coverage within each quadrat was estimated by cropping the mosaic to the area defined by the D-GNSS system for each quadrat. The pixels in the cropped image were then counted and a coverage estimate derived by dividing the number of pixels classed as seagrass by the total number of pixels. This was repeated for each quadrat.

Bootstrapping was used to explore the variation between estimated and observed coverage within quadrats at both sites. This enabled the investigation of classification performance by describing over- or under-estimation of seagrass coverage. Firstly, the difference between estimated and observed percent coverage was calculated for each of the 27 quadrats. Then, a random selection (n=27) of these differences was selected (with replacement enabled, meaning quadrats could be chosen more than once in each iteration) and the mean and standard deviation calculated from the selection. These statistics were stored and the process was then repeated for 1000 iterations, resulting in a selection of 1000 sets of mean, standard deviation and iteration standard error (equal to standard deviation divided by √27) per site. From these, three overall statistics were calculated: the mean and standard deviation of the 27 measured differences, and the overall standard error as the standard deviation of iteration means. The combined uncertainty was then calculated both for each iteration and in total with the following equation:

$$uncertainty = \sqrt{m^2 + \sigma^2 + se^2}$$

where *m* is the mean, σ is the standard deviation and *se* is the standard error.

2.6. Feature Detection

To test the effect of the spatial resolution of the data on the ability to resolve biotic features other than seagrass in intertidal meadows, samples from the mosaics were rescaled to difference spatial resolutions. This was performed using the gdalUtils package (Greenberg and Mattiuzzi, 2015) in R (R Core Team, 2016). The ‘gdalwarp’ function was used to output at resolutions 2,4,6,8 and 10 times coarser than the native

resolution of 4.36 mm pixel^{-1}. The output pixel values were calculated as the mean of the corresponding input pixels.

2.7. Quadrat Sampling Bias

A further analysis exploring the potential biases in quadrat sampling using photos taken at the time of data collection was also conducted. The methods and results of this procedure are presented in the supplementary information (sections 1.3 & 2.1).

3. Results

Data collection at Angle Bay yielded 220 useable images during a flight that lasted 10'57''. At Garron Pill, 191 useable images were collected during a flight 08'43'' in length. Upon visual inspection that stitching had worked, the mosaics were then cropped so that ground control targets and associated tape measures were not included in the imagery, reducing complications during the classification phase (Figs. 3 & 4). Mosaics for both sites had a ground resolution of 4.31 mm pixel^{-1} with a re-projection error (calculated by the software) of 0.32 pixels at both sites. Please see the supplementary information for full processing reports produced by Agisoft Photoscan.

For the RGB classifications optimum classifications were as follows: Angle Bay optical – four classes, two of which were combined for the seagrass class, Garron Pill optical – five classes, one assigned as seagrass. Contrast, dissimilarity and variance were combined with optical data for Angle Bay, and classified with five discreet classes. Three of these were labelled as seagrass. For Garron Pill, contrast, homogeneity and second moment were the optimum texture layers along with the RGB data. Two of the five classes in the optimum classification were combined to make a seagrass class. For the OBIA analysis the combined RGB and texture layers described here were used. Thematic maps showing these classifications can be found in the supplementary information (section 2.2).

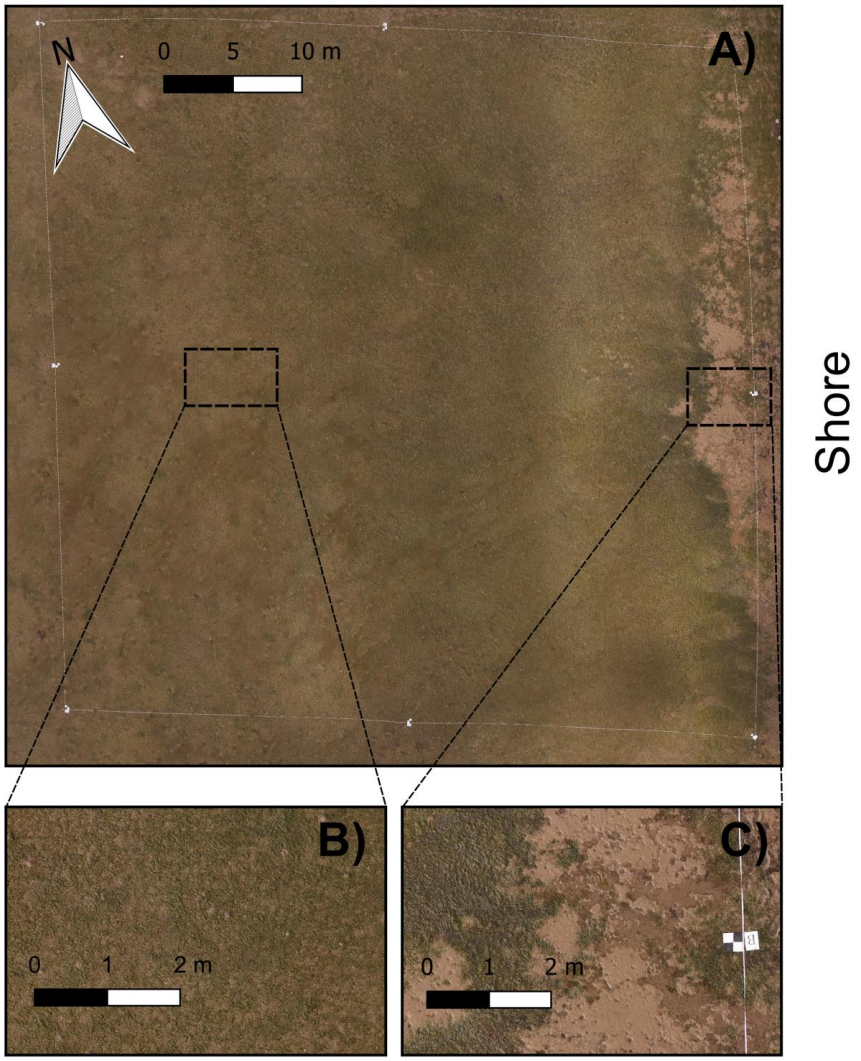

315

316 **Figure 3: Mosaicked RGB imagery of *Zostera noltii* habitat in Angle Bay. The 50x50 m plot is show in A), with two finer**
317 **spatial scale examples shown in B) and C). [COLOUR]**

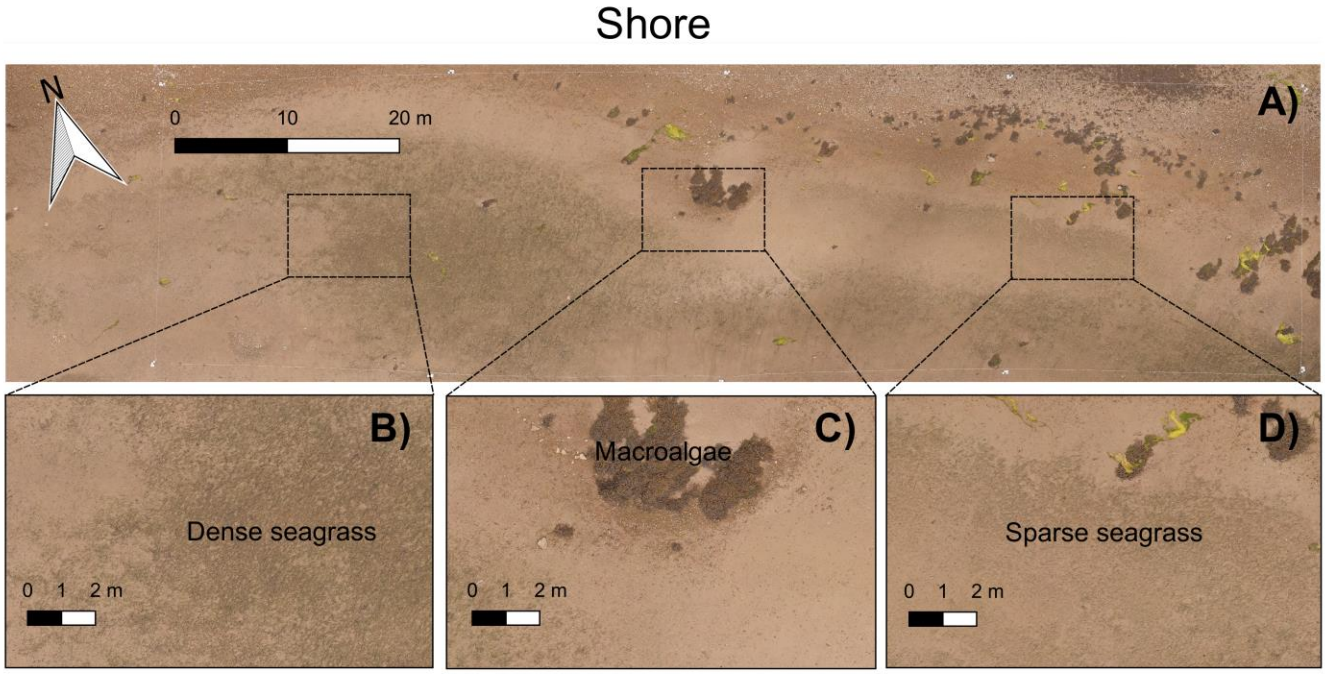

Figure 4: Mosaicked RGB imagery of *Zostera noltii* habitat at Garron Pill. The ~25x100m plot is shown in A), with three finer spatial scale examples shown in B), C) and D). [COLOUR]

The RMSD values calculated from classifications on the data from Garron Pill were all lower than their corresponding results for Angle Bay (Table 1). For Angle Bay, the addition of texture layers increased the RMSD by 5.7 with units of % coverage and SD by 4.3% (i.e. the fit was poorer), whereas for Garron Pill, RMSD was reduced by 0.2% and SD by 0.5%. Object based image analysis did not improve on either of the RGB or RGB & Texture classifications at either site with RMSD and SD values generally much higher. For both of the unsupervised classifications, both under- and overestimations were seen across the 27 quadrats (Fig.5A and 5B), whereas for OBIA, it appears the majority of quadrats were overestimated by the classifier (Fig. 5C). Additionally, quadrat sampling bias was explored, and a mean difference of 15% between observed and classified ground-based photos was found (Figure S1).

The bootstrapped overall uncertainty values show relatively little variation in the unsupervised classifications with and without texture for Garron Pill (Fig. 6). Angle Bay, the more densely vegetated of the two meadows had over double the mean overall uncertainty when compared to Garron Pill for the RGB & texture classification (Table 1). Along with the high RMSD and SD values, the OBIA classifications also showed both high mean overall uncertainty, (the highest being 33% for Angle Bay).

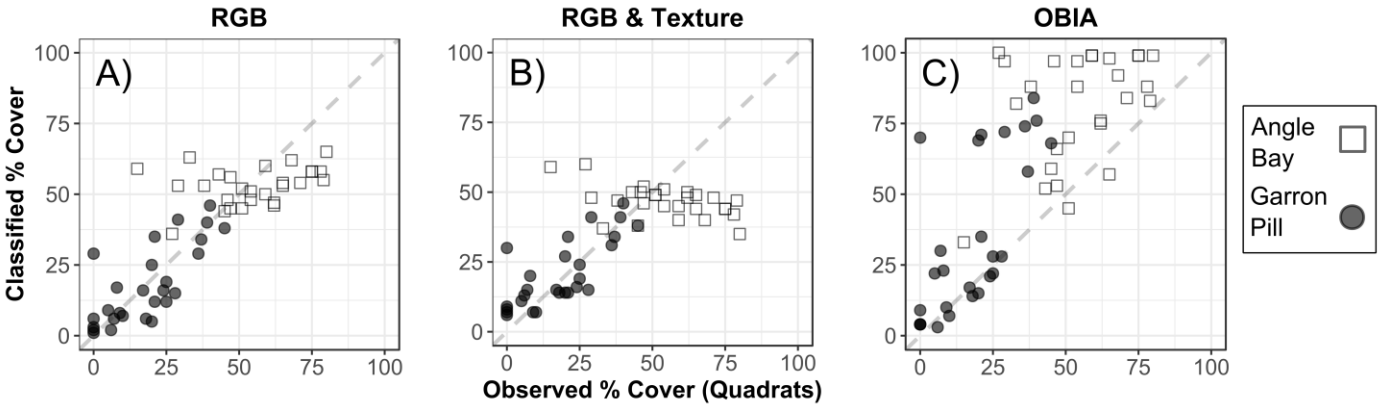

Figure 5: The relationship between observed and classified seagrass coverage observed within quadrats. Unsupervised classifications with red, green and blue bands shown in A), with added texture layers in B) and supervised object-based image analysis results are shown in C).

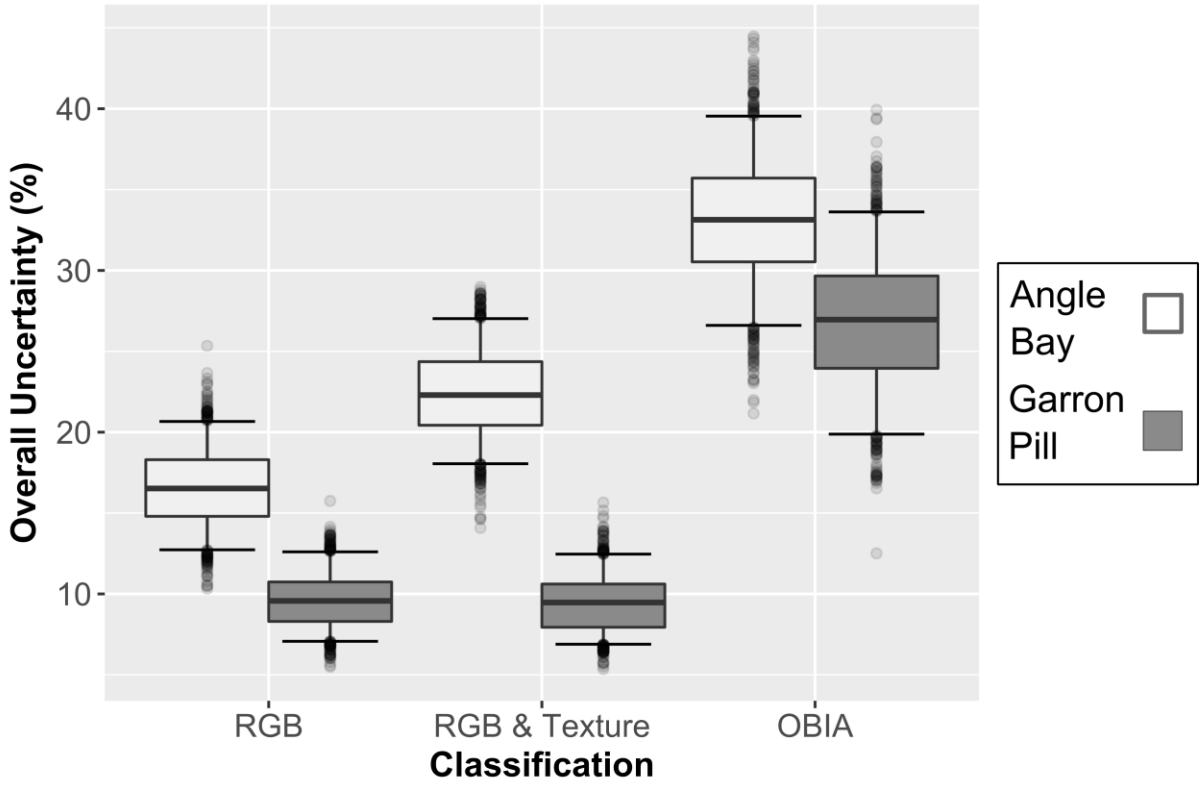

Figure 6: Box and whisker plots showing the distribution of bootstrapped overall uncertainty calculations (n=1000), calculated from the differences between observed and classified seagrass cover in quadrats. Lower and upper hinges refer to 25% and 75% percentiles respectively. Central lines represent the median, whiskers represent 5% and 95% quantiles and points represent outliers.

3.1. Areal Coverage and Perimeter Estimates

Combining the known ground sampling distances (4.36mm) in the orthomosaics with counts of pixels in each classified raster allowed for seagrass areal coverage estimates to be made. For Angle Bay, estimates ranged from 1110 m^2 (47 % of the surveyed areas) produced by the RGB & texture classification to 1967 m^2 (83%)

351 calculated from the OBIA classification (Table 1). Overall, Garron Pill had smaller estimations with the lowest
352 at 555 m^2 (22%) and highest at 904 m^2 (36%) produced with data from the OBIA classifier. OBIA
353 classifications at both sites resulted in greater numbers of pixels being labelled as seagrass, which in turn
354 has driven the higher areal coverage estimates. The two flights at 50m altitude used to collect data from the
355 river channel area yielded total of 258 useable images. These flights were 11' 45'' and 12' 01'' in duration.
356 No ground control points were deployed or used here due to the inaccessibility of the river channel by foot.
357 The images collected were then stitched with the same procedure mentioned earlier in this manuscript, but
358 without the inclusion of GCPs, so therefore relying on GNSS information from the flight log (tagged to images)
359 to produce a georeferenced orthomosaic (Fig. 7). The resulting image demonstrates the capability of this
360 form of data collection to visualise the boundaries of seagrass meadows in terrain that is not accessible by
361 foot (e.g. soft muddy intertidal river beds). Other broad -category vegetation features such as macroalgae
362 are also detectable in these data (Fig. 7C).

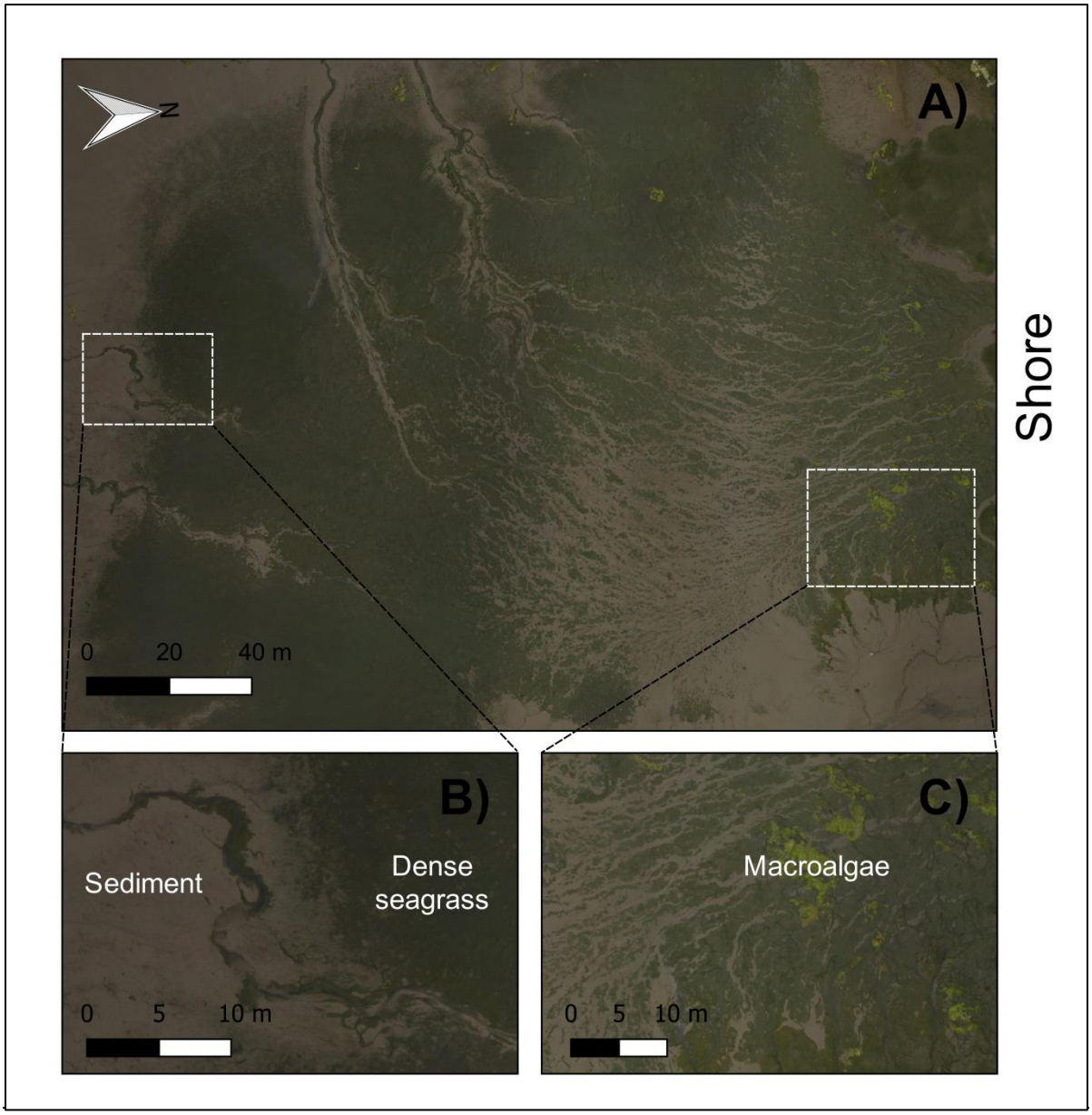

Figure 7: Orthomosaic of *Zostera noltii* meadow boundary at Garron Pill. Images captured at 50m altitude. No ground control targets were deployed at this site due to the inaccessible nature of the river channel. [COLOUR]

3.3. Feature Detection

Within intertidal seagrass meadows, some features can be detected with optical remote sensing data indicating the presence of biotic features other than seagrass that co-habit these environments. At both sites cockles (*Cerastoderma edule)* and Lugworm (*Arenicola sp.*) mounds were found on the sediment surface in high abundance. Fig. 8 displays three example features both at native and multiple resampled resolutions. Lugworm mounds are generally round features approximately 50 – 100 mm in diameter. They were clearly visible at the native resolution in the data and remained detectable even at 43mm pixel^{-1} (× 10) spatial resolution. Cockles on sediment appeared more detectable than those within seagrass (Fig. 8). The shells

remained detectable in the absence of seagrass when viewed at 43 mm pixel^{-1} spatial resolution, but when found within *Zostera noltii* shoots they become undetectable at 17.2 mm pixel^{-1} (× 4) spatial resolution (Fig. 8).

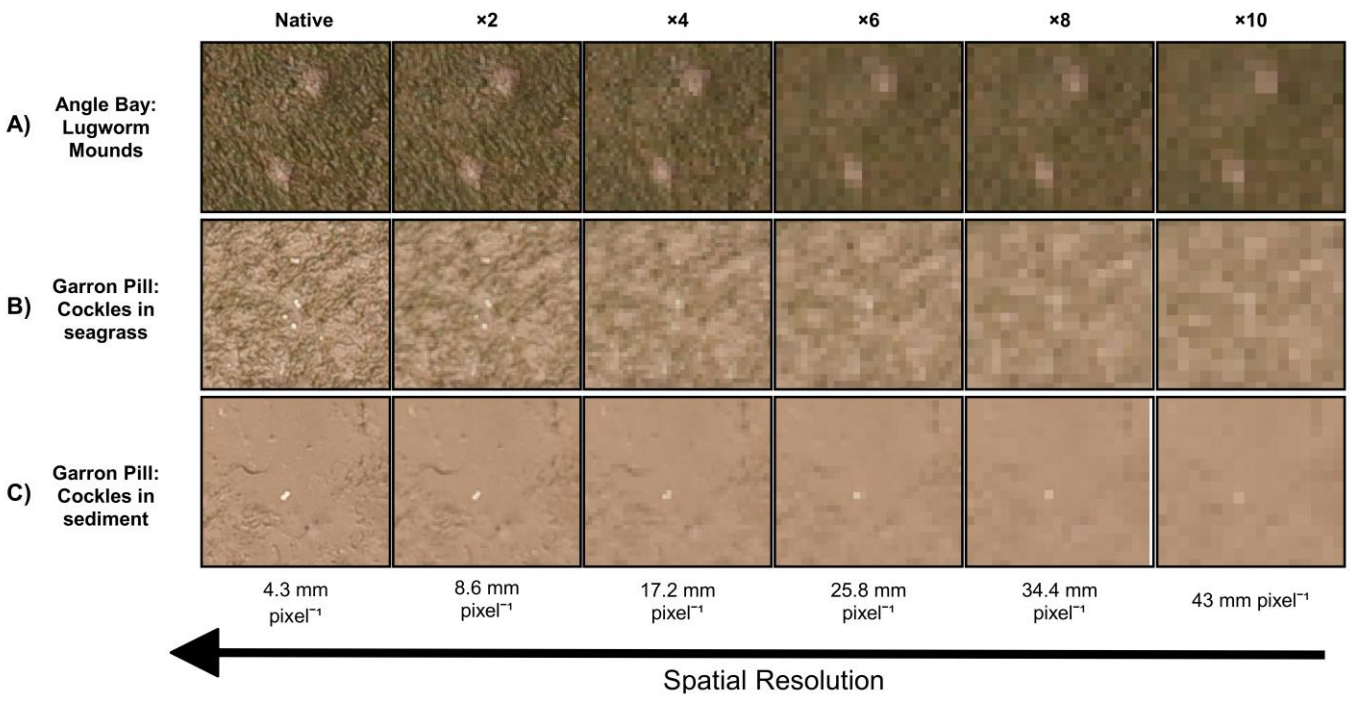

Figure 8: Figure 8: Three examples of ecological features found in *Zostera noltii* meadows. A) Shows two Lugworm (*Arenicola sp.*) mounds, B) Cockle (*Cerastoderma edule)* shells surrounded by seagrass shoots and C) on non-vegetated substrate. [COLOUR]

4. Discussion

This study describes for the first time an approach to intertidal seagrass mapping using a lightweight drone to obtain very fine grained, high spatial resolution data. We found wide variation between classifications when measuring the differences between classified and observed cover within the quadrat samples collected (Table 1). Given that the addition of texture layers has improved classification accuracy in the past in similar habitats such as salt marsh (Kim et al., 2011), we expected to see reduced RMSD scores in this study. It may be that the classification of the very fine spatial resolution data shown in this study can only be improved by the addition of more spectral (e.g. near infra-red) rather than textural layers. The spectral complexity found in hyperspectral optical remote sensing studies on *Zostera noltii* leaves (Bargain et al., 2013) suggests that the addition of further spectral bands may produce a better discrimination between seagrass shoots and background sediment. Different texture measures were selected during the layer selection phase for each

site. This highlights the importance of treating each mosaic individually when selecting layers to input to a classification scheme. Variables such as the spatial resolution of the images, and the meteorological conditions (e.g. cloud cover) during data collection can strongly influence the type of data collected, and in turn which texture measures may highlight differences between seagrass and non-seagrass features.

OBIA has been increasingly employed to analyse fine grained data such as that collected from sensors on board drones (e.g. Husson et al., 2016 and Ventura et al., 2016). In this case, the unsupervised classifications performed better than the support vector machine algorithms used on the segmented data. Despite the very high spatial resolution of the data, *Zostera noltii* shoots still appear as very fine and complex features within the input bands. The segmentation process applied struggled to properly define the edges between seagrass and non-seagrass features, and therefore non-vegetated areas were also captured within the objects labelled as seagrass. This over-estimation is reflected in the comparisons with quadrat data at both sites (Fig. 5). Furthermore, OBIA is notoriously subjective and its poor performance in this scenario may have been caused by the choice of 'training' segments during pre-classification. New segmentation algorithms (e.g. SLIC super pixels; Csillik, 2017), are emerging and in future as these mature, there may be promise to further test these on fine spatial resolution intertidal orthomosaics.

4.1. Coverage Estimates & Assessment of Quadrat Sampling

The variation in coverage estimates produced from the classified data in this study is caused by uncertainty in the classifications themselves. Working at such fine spatial scales allows for the consideration of within-meadow variation and in turn more representative predictions of overall coverage. However, working at such fine spatial scales brings new challenges for data interpretation. Underestimation, seen more commonly for quadrats at Angle Bay (Fig. 5) could be due to the high density of seagrass in parts of this site and the differences between what a sensor captures and what a human observer interprets. This could be caused by a saturation effect also seen in optical remote sensing studies of other vegetated ecosystems (Mutanga et al., 2012). Positive bias, seen in some quadrats at both sites, could potentially be explained by an observer effect. Estimations of coverage by a human observer could take into consideration the fact that seagrasses stand vertically when suspended in water, whereas a sensor, in this case on board a lightweight drone, simply counts the proportion of pixels covered by seagrass. The hypothesis that observer bias was present during ground-based sampling was investigated by examining photographs of the quadrats (see supplementary

information; Fig. S1). Observer bias and variability of cover estimations, regardless of experience, has been raised as an issue with quadrat sampling in terrestrial systems (Sykes et al., 1983). It may be the case that in this study similar issues were causing underestimation, combined with the knowledge that a given number of seagrass shoots change their coverage of a quadrat when suspended in water compared to laid flat at low tide. Although ground based photographs were taken in this study, their quality was variable, and therefore we recommend a standardised approach (i.e. using a fixed height (Luscier et al., 2006) in future investigations.

4.2. Meadow Boundary Detection

Meadow boundaries were clearly visible in the mosaic created with images captured at 50 m altitude. Information of this type provides a cost-effective approach to *Zostera noltii* meadow mapping, especially in tidal channels were the logistics of boat or hovercraft surveying are non-trivial. The distinction between seagrass and macroalgae was clearly visible in the resulting orthomosaic (Fig. 7C), which from a management point of view provides a useful tool to quantify the invasion of other species such as macroalgae in seagrass-dominated habitats (Thomsen et al., 2012).

4.3. Feature Detection

The very fine spatial resolution data produced in this study (4.36 mm pixel^{-1}) allowed for the identification of meadow features such as lugworm (*Arenicola sp.*) mounds and cockle shells (*Cerastoderma edule*). The ability to capture this information within images containing seagrass shoots could allow questions regarding lugworm presence/density effects on *Zostera noltii* density to be revisited (Philippart and Dijkema, 1995). The presence of bivalve shells is also a crude but useful indicator of the health and diversity of the below-surface intertidal environment (Lohrer et al., 2016). With regards to the spatial resolution of the data captured in this study, these features were all identifiable at coarser resolutions than the native data. This indicates that a higher- altitude flight could be conducted resulting in a coarser ground sampling distance, therefore allowing for data collection from a larger area without compromising the ability to capture fine scale biotic features.

In future work, other users should consider monitoring conditions. In this study, conditions were generally overcast and therefore favourable when collecting imagery at Garron Pill, but for Angle Bay, the meteorological conditions were mixed with intermittent sunshine amongst the cloud. As the drone flew with a

variable heading, the sensors viewing angle changed in relation to the sun's position on alternate legs of the drone's way-pointed path (Fig. 1C&D). As a result, the attitude of the drone and therefore the attached sensor, manipulated the presence of glint and shadow in the imagery. Due to the gridded pattern of flight, artefacts have developed at overlapping areas between images during the image stitching process. We recommend in future, to conduct flights with a constant heading, to ensure the sensors view angle remains fixed in relation to sun angle. We would also encourage other users to consider image calibration if time-series monitoring is being undertaken.

4.5. Ecosystem Dynamics and Blue Carbon

The potential of coastal ecosystems and more specifically the plants that live within them to capture and sequester carbon (known as blue carbon) has been a growing field of scientific research (Fourqurean et al., 2012; Macreadie et al., 2014). The coverage estimates that we present here can be complementary to allometric data such as above- and below-ground biomass calculations to ultimately produce more accurate estimations. This has been demonstrated in terrestrial systems with drone-based data (Cunliffe et al., 2016). This can then be combined with information about carbon capture in a particular species such as *Zostera noltii*, quantifying the amount of carbon stored in a given meadow and allowing its monetary value to be estimated. Monetary valuation such as this is likely to give great value to policy decision making (Turner et al., 2003). Aside from monetary valuation, fine-scale data such as these can potentially improve the performance of predictive habitat modelling approaches which have been applied to understand seagrass distribution (Grech and Coles, 2010).

For another species of seagrass, seasonality has been shown to create changes of up to 35% in coverage estimates of seagrass meadows on the coast of Reunion Island (Cuvillier et al., 2016). *Zostera noltii* is a perennial species that grows in spring and summer, flowers, and then dies back to about half its peak density in autumn and winter (Auby and Labourg, 1996). While this variation in above ground biomass is an issue with ground based surveying (Mckenzie et al., 2003), using drones with user-dictated data collection, allows for repeatable data collection at the same stage of the annual phenological cycle of a seagrass species such as this. The case for repeat studies at the same time of year is also strengthened by the discovery of a seasonal variation in pigment concentration in *Zostera noltii* leaves, which in turn can influence measurements derived from remote sensing products (Bargain et al., 2013).

5. Conclusions

In this study we have demonstrated the potential of low-cost, flexible, drone-based data collection techniques for monitoring intertidal seagrass meadows. Working on foot in an intertidal environment can be challenging and one clear advantage of drone technology is the flexibility in deployment and the utility of data, as we have demonstrated here. Time-series monitoring is critical to understand the dynamics of seagrass meadows, especially when it comes to disentangling the natural variation from changes that are human-induced (Cunha et al., 2005).

The understanding of within-meadow seagrass heterogeneity is a complementary approach to more traditional boundary mapping which has often been conducted using satellite and airborne imagery (e.g. Phinn et al., 2008). Drones bring the ability to capture data useful for within environment variation analysis, which has also been demonstrated in wetlands (Zweig et al., 2015). With threats such as reduced water quality and wasting disease, the decline in meadow quality may be more nuanced than a simple shrinking in overall extent, highlighting the need to understand the more complex matrix of plants and sediment in the intertidal environment. It is therefore crucial to investigate the fragmentation within meadows, which can inform researchers and managers whether a meadow is potentially degrading or recovering. The combination of this previously unobtainable data and the cost-effective, self-service nature of drone based remote sensing gives great promise to the application of drones for seagrass conservation efforts.

Moving forward, we feel that the rapidly developing field of lightweight drones and miniaturisation of sensors for optical remote sensing will soon allow for more detailed measurements of meadow quality such as plant health and presence of wasting disease based on the spectral signatures obtained from seagrass shoots.

6. Tables

Table 1: Accuracy assessment of unsupervised classifications including both RGB and RGB and Texture, and OBIA classifications. Root mean squared deviation (RMSD) and standard deviation (SD) and bias calculated on the percentage difference between observed and classified seagrass cover in quadrats. Bootstrapped SE was calculated in the bootstrapping process. Overall uncertainty calculated from bias, SD and bootstrapped SE using the equation described in section 2.5.4. Coverage estimates calculated by totalling the number of pixels classed as seagrass at each site.

Site	Layers	No. Classes	RMSD (%)	SD	Bias (%)	Bootstrapped SE	Overall Uncertainty	Estimated Coverage (m^2)	Estimated Coverage (%)
Angle Bay	RGB	4	16.12	16.33	-1.78	0.5	16.71	1224.07	51.93
	RGB & Texture	5	21.85	20.65	-8.19	0.63	22.54	1110.33	47.10
	RGB & Texture (OBIA)	2	32.74	20.53	25.81	0.63	33.2	1967.14	83.45
Garron Pill	RGB	5	9.45	9.62	-0.4	0.29	9.8	554.92	21.86
	RGB & Texture	5	9.22	9.06	2.44	0.28	9.54	661.77	26.07
	RGB & Texture (OBIA)	5	26.42	20.95	16.59	0.65	27.01	904.35	35.62

Acknowledgements

We would like to thank Benjamin Leutner, Moritz Lennert and Chris Kay-Ayling for assistance with the analysis of this data. We are grateful to two anonymous reviewers whose advice and comments helped improve this work. This work was supported by the Natural Environment Research Council [grant number 570009815 to JPD].

References

Agisoft LLC, 2016. Photoscan Professional (1.2.5).

Anderson, K., Gaston, K.J., 2013. Lightweight unmanned aerial vehicles will revolutionize spatial ecology. Front. Ecol. Environ. 11, 138–146. doi:10.1890/120150

Auby, I., Labourg, P., 1996. Seasonal Dynamics of Zostera Noltii Hornem. In The Bay of Arcachon (France). J. Sea Res. 35, 269–277. doi:http://dx.doi.org/10.1016/S1385-1101(96)90754-6

Auguie, B., 2016. gridExtra: Miscellaneous Functions for "Grid" Graphics.

Barbier, E.B., Hacker, S.D., Kennedy, C.J., Koch, E.W., Stier, A.C., Silliman, B.R., 2011. The value of estuarine and coastal ecosystem services. Ecol. Monogr. 81, 169–193. doi:10.1890/10-1510.1

Bargain, A., Robin, M., Méléder, V., Rosa, P., Menn, E.L., Harin, N., Barillé, L., 2013. Seasonal spectral variation of Zostera noltii and its influence on pigment-based Vegetation Indices. J. Exp. Mar. Bio. Ecol. 446, 86–94. doi:10.1016/j.jembe.2013.04.012

Barrell, J., Grant, J., Hanson, A., Mahoney, M., 2015. Evaluating the complementarity of acoustic and satellite remote sensing for seagrass landscape mapping. Int. J. Remote Sens. 36, 4069–4094. doi:10.1080/01431161.2015.1076208

526 Baumstark, R., Duffey, R., Pu, R., 2016. Mapping seagrass and colonized hard bottom in Springs Coast ,
527 Florida using WorldView-2 satellite imagery. Estuar. Coast. Shelf Sci. 181, 83–92.
528 doi:10.1016/j.ecss.2016.08.019

529 Beaumont, N.J., Austen, M.C., Mangi, S.C., Townsend, M., 2008. Economic valuation for the conservation
530 of marine biodiversity 56, 386–396. doi:10.1016/j.marpolbul.2007.11.013

531 Bernard, G., Boudouresque, C.F., Picon, P., 2007. Long term changes in Zostera meadows in the Berre
532 lagoon (Provence, Mediterranean Sea). Estuar. Coast. Shelf Sci. 73, 617–629.
533 doi:10.1016/j.ecss.2007.03.003

534 Bertelli, C.M., Robinson, M.T., Mendzil, A.F., Pratt, L.R., Unsworth, R.K.F., 2017. Finding some seagrass
535 optimism in Wales , the case of Zostera noltii. Mar. Pollut. Bull. doi:10.1016/j.marpolbul.2017.08.018

536 Bertelli, C.M., Unsworth, R.K.F., 2014. Protecting the hand that feeds us: Seagrass (Zostera marina)
537 serves as commercial juvenile fish habitat. Mar. Pollut. Bull. 83, 425–429.
538 doi:10.1016/j.marpolbul.2013.08.011

539 Blaschke, T., 2010. Object based image analysis for remote sensing. ISPRS J. Photogramm. Remote
540 Sens. 65, 2–16. doi:10.1016/j.isprsjprs.2009.06.004

541 Cabaço, S., Cabaço, S., Santos, R., 2007. Effects of burial and erosion on the seagrass Zostera noltii. J.
542 Exp. Mar. Bio. Ecol. 340, 204–212. doi:10.1016/j.jembe.2006.09.003

543 Chabot, D., Craik, S.R., Bird, D.M., 2015. Population census of a large common tern colony with a small
544 unmanned aircraft. PLoS One 10, e0122588. doi:10.1371/journal.pone.0122588

545 Chirayath, V., Earle, S.A., 2016. Drones that see through waves – preliminary results from airborne fluid
546 lensing for centimetre-scale aquatic conservation. Aquat. Conserv. 26, 237–250.
547 doi:10.1002/aqc.2654

548 Csillik, O., 2017. Fast Segmentation and Classification of Very High Resolution Remote Sensing Data
549 Using. Remote Sens. 9. doi:10.3390/rs9030243

550 Cunha, A.H., Santos, R.P., Gaspar, A.P., Bairros, M.F., 2005. Seagrass landscape-scale changes in
551 response to disturbance created by the dynamics of barrier-islands: A case study from Ria Formosa
552 (Southern Portugal). Estuar. Coast. Shelf Sci. 64, 636–644. doi:10.1016/j.ecss.2005.03.018

553 Cunliffe, A.M., Brazier, R.E., Anderson, K., 2016. Ultra-fine grain landscape-scale quantification of dryland
554 vegetation structure with drone-acquired structure-from-motion photogrammetry. Remote Sens.
555 Environ. 183, 129–143. doi:10.1016/j.rse.2016.05.019

556 Cuvillier, A., Villeneuve, N., Cordier, E., Kolasinski, J., Maurel, L., Farnier, N., Frouin, P., 2016. Causes of
557 seasonal and decadal variability in a tropical seagrass seascape (Reunion Island, South Western
558 Indian Ocean). Estuar. Coast. Shelf Sci. 184, 90–101. doi:10.1016/j.ecss.2016.10.046

559 Dandois, J., Olano, M., Ellis, E., 2015. Optimal Altitude, Overlap, and Weather Conditions for Computer
560 Vision UAV Estimates of Forest Structure. Remote Sens. 7, 13895–13920. doi:10.3390/rs71013895

561 DeBell, L., Anderson, K., Brazier, R.E., King, N., Jones, L., 2015. Water resource management at
562 catchment scales using lightweight UAVs : current capabilities and future perspectives. J. Unmanned
563 Veh. Syst. 30, 7–30.

564 Duarte, C.M., 2002. The future of seagrass meadows. Environ. Conserv. 29, 192–206.
565 doi:10.1017/S0376892902000127

566 Fourqurean, J.W., Duarte, C.M., Kennedy, H., Marbà, N., Holmer, M., Mateo, M.A., Apostolaki, E.T.,
567 Kendrick, G.A., Krause-Jensen, D., McGlathery, K.J., Serrano, O., 2012. Seagrass ecosystems as a
568 globally significant carbon stock. Nat. Geosci. 5, 505–509. doi:10.1038/ngeo1477

569 Gonçalves, J.A., Henriques, R., 2015. UAV photogrammetry for topographic monitoring of coastal areas.
570 ISPRS J. Photogramm. Remote Sens. 104, 101–111. doi:10.1016/j.isprsjprs.2015.02.009

571 Gotceitas, V., Fraser, S., Brown, J.A., 1997. Use of eelgrass beds (*Zostera marina*) by juvenile Atlantic cod
572 (*Gadus morhua*). Can. J. Fish. Aquat. Sci. 54, 1306–1319. doi:10.1139/f97-033

573 GRASS Development Team, 2015. Geographic Resources Analysis Support System (GRASS) 7.0.

574 Grech, A., Coles, R.G., 2010. An ecosystem-scale predictive model of coastal seagrass distribution. Aquat.
575 Conserv. Mar. Freshw. Ecosyst. 20, 437–444. doi:10.1002/aqc.1107

576 Greenberg, J.A., Mattiuzzi, M., 2015. gdalUtils: Wrappers for the Geospatial Data Abstraction Library
577 (GDAL) Utilities.

578 Gross, J.W., Heumann, B.W., 2016. A Statistical Examination of Image Stitching Software Packages For
579 Use With Unmanned Aerial Systems. Photogramm. Eng. Remote Sens. 82, 419–425.
580 doi:10.14358/PERS.82.6.419

581 Han, Q., Bouma, T.J., Brun, F.G., Suykerbuyk, W., Katwijk, M.M. Van, 2012. Resilience of Zostera noltii to
582 burial or erosion disturbances. Mar. Ecol. Prog. Ser. 449, 133–143. doi:10.3354/meps09532

583 Haralick, R.M., Shanmugam, K., Dinstein, I., 1973. Textural Features for Image Classification. IEEE Trans.
584 Syst. Man. Cybern. 3, 610–621. doi:10.1109/TSMC.1973.4309314

585 Hartigan, J.A., Wong, M.A., 1979. Algorithm AS 136: A K-Means Clustering Algorithm. J. R. Stat. Soc. Ser.
586 C (Applied Stat. 28, 100–108. doi:10.2307/2346101

587 Hernandez, I., Peralta, G., Perez-Llorens, J.L., Vergara, J.J., 1997. Biomass and Dynamics of Growth of
588 Ulva Species in Palmones River Estuary. J. Phycol. 33, 764–772. doi:10.1111/j.0022-
589 3646.1997.00764.x

590 Hijmans, R.J., 2015. raster: Geographic Data Analysis and Modeling. R package version 2.5-2.

591 Hodgson, A., Kelly, N., Peel, D., 2013. Unmanned aerial vehicles (UAVs) for surveying Marine Fauna: A
592 dugong case study. PLoS One 8, e79556. doi:10.1371/journal.pone.0079556

593 Hossain, M.S., Bujang, J.S., Zakaria, M.H., Hashim, M., 2014. The application of remote sensing to
594 seagrass ecosystems: an overview and future research prospects. Int. J. Remote Sens. 36, 61–114.
595 doi:10.1080/01431161.2014.990649

596 Husson, E., Ecke, F., Reese, H., 2016. Comparison of Manual Mapping and Automated Object-Based
597 Image Analysis of Non-Submerged Aquatic Vegetation from Very-High-Resolution UAS Images.
598 Remote Sens. 8, 724. doi:10.3390/rs8090724

599 Huya-Kouadio, F., 2016. Tower.

600 Inoue, T., Nagai, S., Yamashita, S., Fadaei, H., Ishii, R., Okabe, K., Taki, H., Honda, Y., Kajiwara, K.,
601 Suzuki, R., 2014. Unmanned Aerial Survey of Fallen Trees in a Deciduous Broadleaved Forest in
602 Eastern Japan. PLoS One 9, e109881. doi:10.1371/journal.pone.0109881

603 Jones, B.L., Unsworth, R.K.F., 2016. The perilous state of seagrass in the British Isles. R. Soc. Open Sci.
604 3, 1–14. doi:http://dx.doi.org/10.1098/rsos.150596

605 Kay, S., Hedley, J.D., Lavender, S., 2009. Sun Glint Correction of High and Low Spatial Resolution Images
606 of Aquatic Scenes: a Review of Methods for Visible and Near-Infrared Wavelengths. Remote Sens. 1,
607 697–730. doi:10.3390/rs1040697

608 Kim, M., Warner, T.A., Madden, M., Atkinson, D.S., Kim, M., Warner, T.A., Madden, M., Atkinson, D.S.,
609 Kim, M., Warner, T.A., Madden, M., Atkinson, D.S., 2011. Multi-scale GEOBIA with very high spatial
610 resolution digital aerial imagery : scale , texture and image objects. Int. J. Remote Sens. 32, 2825–
611 2850. doi:10.1080/01431161003745608

612 Knudby, A., Newman, C., Shaghude, Y., Muhando, C., 2010. Simple and effective monitoring of historic
613 changes in nearshore environments using the free archive of Landsat imagery. Int. J. Appl. Earth Obs.
614 Geoinf. 12, 116–122. doi:10.1016/j.jag.2009.09.002

615 Lamb, J.B., Water, J.A.J.M. Van De, Bourne, D.G., Altier, C., Hein, M.Y., Fiorenza, E.A., Abu, N., Jompa,
616 J., Harvell, C.D., 2017. Seagrass ecosystems reduce exposure to bacterial pathogens of humans,
617 fishes, and invertebrates. Science (80-.). 355, 731–733.

618 Leutner, B., Horning, N., 2016. RStoolbox: Tools for Remote Sensing Data Analysis. R package version
619 0.1.4.9000.

620 Lohrer, A.M., Townsend, M., Hailes, S.F., Rodil, I.F., Cartner, K., Pratt, D.R., Hewitt, J.E., 2016. Influence
621 of New Zealand cockles (Austrovenus stutchburyi) on primary productivity in sandflat-seagrass
622 (Zostera muelleri) ecotones. Estuar. Coast. Shelf Sci. 181, 238–248. doi:10.1016/j.ecss.2016.08.045

623 Luscier, J.D., Thompson, W.L., Wilson, J.M., Gorham, B.E., Dragut, L.D., 2006. Using digital photographs

624 and object-based image analysis to estimate percent ground cover in vegetation plots. Front. Ecol.
625 Environ. 4, 408–413. doi:10.1890/1540-9295(2006)4[408:UDPAOI]2.0.CO;2

626 Lyons, M., Roelfsema, C., Kovacs, E., Samper-Villarreal, J., Saunders, M., Maxwell, P., Phinn, S., 2015.
627 Rapid monitoring of seagrass biomass using a simple linear modelling approach, in the field and from
628 space. Mar. Ecol. Prog. Ser. 530, 1–14. doi:10.3354/meps11321

629 Macreadie, P.I., Baird, M.E., Trevathan-Tackett, S.M., Larkum, A.W.D., Ralph, P.J., 2014. Quantifying and
630 modelling the carbon sequestration capacity of seagrass meadows – A critical assessment. Mar.
631 Pollut. Bull. 83, 430–439. doi:10.1016/j.marpolbul.2013.07.038

632 Marbà, N., Duarte, C.M., 2010. Mediterranean warming triggers seagrass (Posidonia oceanica) shoot
633 mortality. Glob. Chang. Biol. 16, 2366–2375. doi:10.1111/j.1365-2486.2009.02130.x

634 Martins, I., Neto, J.M., Fontes, M.G., Marques, J.C., Pardal, M.A., 2005. Seasonal variation in short-term
635 survival of Zostera noltii transplants in a declining meadow in Portugal. Aquat. Bot. 82, 132–142.
636 doi:10.1016/j.aquabot.2005.03.006

637 McGlathery, K.J., Reynolds, L.K., Cole, L.W., Orth, R.J., Marion, S.R., Schwarzschild, A., 2012. Recovery
638 trajectories during state change from bare sediment to eelgrass dominance. Mar. Ecol. Prog. Ser. 448,
639 209–221. doi:10.3354/meps09574

640 Mckenzie, L.J., 2003. Guidelines for the rapid assessment of seagrass habitats in the western Pacific.

641 Mckenzie, L.J., Campbell, S.J., Roder, C.A., 2003. Seagrass-Watch: Manual for Mapping & Monitoring
642 Seagrass Resources by Community (Citizen) Volunteers.

643 Misbari, S., Hashim, M., 2016. Change Detection of Submerged Seagrass Biomass in Shallow Coastal
644 Water. Remote Sens. 8, 200. doi:10.3390/rs8030200

645 Moore, K.A., Wilcox, D.J., Orth, R.J., 2000. Analysis of the abundance of submersed aquatic vegetation
646 communities in the Chesapeake Bay. Estuaries 23, 115–127. doi:10.2307/1353229

647 Mutanga, O., Adam, E., Azong, M., 2012. High density biomass estimation for wetland vegetation using
648 WorldView-2 imagery and random forest regression algorithm. Int. J. Appl. Earth Obs. Geoinf. 18,
649 399–406. doi:10.1016/j.jag.2012.03.012

650 Myint, S.W., Gober, P., Brazel, A., Grossman-clarke, S., Weng, Q., 2011. Per-pixel vs. object-based
651 classification of urban land cover extraction using high spatial resolution imagery. Remote Sens.
652 Environ. 115, 1145–1161. doi:10.1016/j.rse.2010.12.017

653 Oborne, M., 2016. Mission Planner.

654 Orth, R.J., Carruthers, T.J.B., Dennison, W.C., Duarte, C.M., Fourqurean, J.W., Heck, K.L., Hughes, A.R.,
655 Kendrick, G.A., Kenworthy, W.J., Olyarnik, S., Short, F.T., Waycott, M., Williams, S.L., 2006. A Global

Crisis for Seagrass Ecosystems. Bioscience 56, 987–996. doi:10.1641/0006-3568(2006)56[987:AGCFSE]2.0.CO

Pergent-Martini, C., Buia, M., Fernandez Torquemada, Y., 2015. Zostera noltii. The IUCN Red List of Threatened Species 2015: e.T173361A17475420 [WWW Document].

Philippart, C.J.M., Dijkema, K.S., 1995. Wax and wane of Zostera noltii Hornem. in the Dutch Wadden Sea. Aquat. Bot. 49, 255–268. doi:10.1016/0304-3770(94)00431-K

Phinn, S., Roelfsema, C., Dekker, A., Brando, V., Anstee, J., 2008. Mapping seagrass species, cover and biomass in shallow waters : An assessment of satellite multi-spectral and airborne hyper-spectral imaging systems in. Remote Sens. Environ. 112, 3413–3425. doi:10.1016/j.rse.2007.09.017

R Core Team, 2016. R: A language and environment for statistical computing.

Roelfsema, C.M., Lyons, M., Kovacs, E.M., Maxwell, P., Saunders, M.I., Samper-Villarreal, J., Phinn, S.R., 2014. Multi-temporal mapping of seagrass cover, species and biomass: A semi-automated object based image analysis approach. Remote Sens. Environ. 150, 172–187. doi:10.1016/j.rse.2014.05.001

Ryan, J.C., Hubbard, A.L., Box, J.E., Todd, J., Christoffersen, P., Carr, J.R., Holt, T.O., Snooke, N., 2015. UAV photogrammetry and structure from motion to assess calving dynamics at Store Glacier, a large outlet draining the Greenland ice sheet. Cryosph. 9, 1–11. doi:10.5194/tc-9-1-2015

Short, F.T., Carruthers, T.J.R., Waycott, M., Kendrick, G.A., Fourqurean, J.W., Callabine, A., Kenworthy, W.J., Dennison, W.C., 2010. Zostera noltii. The IUCN Red List of Threatened Species 2010: e.T173361A6999224 [WWW Document]. IUCN Redl List Threat. Species. URL http://www.iucnredlist.org/details/biblio/173361/0 (accessed 11.22.16).

Short, F.T., Polidoro, B., Livingstone, S.R., Carpenter, K.E., Bandeira, S., Bujang, J.S., Calumpong, H.P., Carruthers, T.J.B., Coles, R.G., Dennison, W.C., Erftemeijer, P.L.A., Fortes, M.D., Freeman, A.S., Jagtap, T.G., Kamal, A.H.M., Kendrick, G.A., Judson Kenworthy, W., La Nafie, Y.A., Nasution, I.M., Orth, R.J., Prathep, A., Sanciangco, J.C., Tussenbroek, B. van, Vergara, S.G., Waycott, M., Zieman, J.C., 2011. Extinction risk assessment of the world's seagrass species. Biol. Conserv. 144, 1961–1971. doi:10.1016/j.biocon.2011.04.010

Short, F.T., Wyllie-Echeverria, S., 1996. Natural and human-induced disturbance of seagrasses. Environ. Conserv. 23, 17–27. doi:10.1017/S0376892900038212

Smith, M.W., Carrivick, J.L., Quincey, D.J., 2015. Structure from motion photogrammetry in physical geography. Prog. Phys. Geogr. 40, 1–29. doi:10.1177/0309133315615805

Stekoll, M.S., Deysher, L.E., Hess, M., 2006. A remote sensing approach to estimating harvestable kelp biomass. J. Appl. Phycol. 18, 323–334. doi:10.1007/s10811-006-9029-7

Sterckx, S., Knaeps, E., Ruddick, K., 2011. Detection and correction of adjacency effects in hyperspectral

689 airborne data of coastal and inland waters: the use of the near infrared similarity spectrum. Int. J.
690 Remote Sens. 32, 6479–6505. doi:10.1080/01431161.2010.512930

691 Strahler, A.H., Woodcock, C.E., Smith, J.A., 1986. On the Nature of Models in Remote Sensing. Remote
692 Sens. Environ. 20, 121–139.

693 Suominen, T., Tolvanen, H., 2016. Temporal analysis of remotely sensed turbidity in a coastal archipelago.
694 Int. J. Appl. Earth Obs. Geoinf. 49, 188–199. doi:10.1016/j.jag.2016.01.012

695 Sykes, J.M., Horrill, A.D., Mountford, M.D., 1983. Use of Visual Cover Assessments as Quantitative
696 Estimators of Some British Woodland Taxa. J. Ecol. 71, 437–450. doi:10.2307/2259726

697 Thomsen, M.S., Wernberg, T., Engelen, A.H., Tuya, F., Mat, A., Holmer, M., Mcglathery, K.J., Arenas, F.,
698 Kotta, J., Brian, R., 2012. A Meta-Analysis of Seaweed Impacts on Seagrasses: Generalities and
699 Knowledge Gaps. PLoS One 7, e28595. doi:10.1371/journal.pone.0028595

700 Turner, R.K., Paavola, J., Cooper, P., Farber, S., Jessamy, V., Georgiou, S., 2003. Valuing nature: lessons
701 learned and future research directions. Ecol. Econ. 46, 493–510. doi:10.1016/S0921-8009(03)00189-7

702 Valle, M., Borja, ??ngel, Chust, G., Galparsoro, I., Garmendia, J.M., 2011. Modelling suitable estuarine
703 habitats for Zostera noltii, using Ecological Niche Factor Analysis and Bathymetric LiDAR. Estuar.
704 Coast. Shelf Sci. 94, 144–154. doi:10.1016/j.ecss.2011.05.031

705 Valle, M., Pala, V., Lafon, V., Dehouck, A., Garmendia, J.M., A, B., Chust, G., 2015. Mapping estuarine
706 habitats using airborne hyperspectral imagery, with special focus on seagrass meadows. Estuar.
707 Coast. Shelf Sci. 164, 433–442. doi:10.1016/j.ecss.2015.07.034

708 Ventura, D., Bruno, M., Jona Lasinio, G., Belluscio, A., Ardizzone, G., 2016. A low-cost drone based
709 application for identifying and mapping of coastal fish nursery grounds. Estuar. Coast. Shelf Sci. 171,
710 85–98. doi:10.1016/j.ecss.2016.01.030

711 Waycott, M., Duarte, C.M., Carruthers, T.J.B., Orth, R.J., Dennison, W.C., Olyarnik, S., Calladine, A.,
712 Fourqurean, J.W., Heck, K.L., Hughes, a R., Kendrick, G. a, Kenworthy, W.J., Short, F.T., Williams,
713 S.L., 2009. Accelerating loss of seagrasses across the globe threatens coastal ecosystems. Proc.
714 Natl. Acad. Sci. U. S. A. 106, 12377–12381. doi:10.1073/pnas.0905620106

715 Wickham, H., 2017. tidyr: Easily Tidy Data with “spread()” and “gather()” Functions.

716 Wickham, H., 2009. ggplot2: Elegant Graphics for Data Analysis. Springer-Verlag, New York.

717 Wickham, H., Francois, R., 2016. dplyr: A Grammar of Data Manipulation.

718 Zvoleff, A., 2016. glcm: Calculate Textures from Grey-Level Co-Occurrence Matrices (GLCMs).

719 Zweig, C.L., Burgess, M.A., Percival, H.F., Kitchens, W.M., 2015. Use of Unmanned Aircraft Systems to
720 Delineate Fine-Scale Wetland Vegetation Communities. Wetlands 35, 303–309. doi:10.1007/s13157-

721 014-0612-4

722